PCCP

Electronic spectrum of the anthracene–ammonia complex

Reika Kanya and Yasuhiro Ohshima*

Department of Chemistry, Graduate School of Science, Kyoto University, Kitashirakawa-Oiwakecho, Sakyo-ku, Kyoto 606-8502, Japan. E-mail: ohshima@kuchem.kyoto-u.ac.jp; Fax: +81-75-753-3974

Received 21st May 2003, Accepted 9th July 2003
First published as an Advance Article on the web 8th August 2003

Fluorescence excitation and ultraviolet–ultraviolet hole burning spectra of jet-cooled anthracene–ammonia clusters were observed. The S_1–S_0 origin of the 1 : 1 complex shows doublet bands, which were assigned to those in the ground and the first excited states of the internal rotation associated with the *ortho* and *para* hydrogen nuclear spin states of NH_3, respectively. The ammonia molecule is located above the centre of the aromatic plane with a centre-of-mass distance of 3.6 Å, which is typical of a π hydrogen bonded aromatic complex. The rotational contour of the internal rotation excited state was analyzed with an effective Hamiltonian including the coupling between the internal and end-over-end rotations, to show that the internal rotation angular momentum is partially quenched because of the potential anisotropy for rotation around the axis that connects the centres of mass of ammonia and anthracene.

Introduction

It has been well accepted that weak non-covalent interaction between proton donating species and π electron clouds of aromatic rings, commonly termed as "π hydrogen bond," is an important controlling factor of molecular packing in aromatic crystals, solvation of aromatics into protic solvents, and conformation of biological supramolecules.[1,2] Unequivocal characterization of the π hydrogen bonds has been provided by studies on van der Waals (vdW) complexes of simple proton donors and aromatic hydrocarbons, in which influences from other nearby molecules are eliminated. Spectroscopic investigations of benzene complexed with hydrogen fluoride,[3] hydrogen chloride,[4,5] water,[6–8] ammonia,[9] and hydrogen sulfide[10] has shown that the attaching molecules reside on the aromatic plane with their X–H bonds (X = F, Cl, O, N, or S) pointing toward the ring. The donor's hydrogen atoms are > 2.3 Å above the plane in the complexes, much more distant than in typical hydrogen bonds between strong proton donor and acceptor. Yet, binding energies of benzene–water[11] and –ammonia[12] have been determined as not much smaller than that of a normal hydrogen bond in the water dimer.[13]

Because of the weakness of the π hydrogen bond in the complexes, the proton donor can execute large amplitude translational and librational motions relative to the aromatic plane and the vdW vibrations provide dense and complicated energy levels. In addition, the intermolecular force is often so isotropic that the attached molecule can interconvert among multiple local-minimum orientations or rotate rather freely. Then further complication is introduced as each eigenstate is split into multiplet by quantum tunneling or angular momenta of the internal rotation of the molecule and the end-over-end rotation of the complex are coupled to each other. Experiments to determine the vibration–rotation–tunneling energy levels are indispensable for more detailed evaluation of the π hydrogen bond, but such studies have been reported only for the simplest system, benzene–water. Its rotational spectra in the vibronic ground state were recorded: transitions in the first excited state associating to internal rotation were observed to be as strong as those in the ground internal rotation state.[6–8] Its vibronic spectra pertinent to the benzene S_1–S_0 excitation were studied by resonance two photon ionization (R2PI), and rotational contour analysis of the 6_0^1 band showed the contribution of two overlapping subbands due to internal rotation.[14] Several intermolecular bands built on the O–H stretch vibrations of water were probed by ionization-detected infrared spectroscopy, and an analysis considering two internal degrees of freedom was performed to simulate the spectra.[15] Ionization-detected stimulated Raman spectroscopy was applied to observe intermolecular vibrations in the ground vibronic manifold.[16] A six-dimensional calculation on the intermolecular states of the complex was carried out and the results based on a model potential were compared with the experiments so far reported.[17] Quite recently, the isovalent system, benzene–hydrogen sulfide, was also studied *via* rotational spectroscopy, and transitions in two excited states for internal rotation were identified as well as those in the ground state.[10] For the closely related benzene–ammonia complex, on the other hand, the ground internal rotation subband in the S_1–S_0 6_0^1 transition was only analyzed even though the excited state subbands were observed as being clearly separated in the R2PI spectrum.[9] Also, transitions in the lowest internal rotation state were only reported in the rotational spectrum.[9] R2PI spectra of anthracene–$(H_2O)_n$ were reported, but no analysis was given for the vibronic spectrum of the anthracene–H_2O complex.[18]

Here, we report excitation spectra of the anthracene–ammonia complex pertaining to the origin band of the anthracene S_1–S_0 transition, especially to show details on the coupling between the internal rotation and over-all rotation in the π hydrogen bonded system. Laser induced fluorescence (LIF) spectra of the anthracene–$(ammonia)_n$ clusters were first reported by Anner and Haas.[19] They observed two types of spectral features, sharp bands with relatively small red shifts which exhibit almost resonant fluorescence and largely red-shifted broad bands which represent Stokes emission, but their carriers were not confirmed. In the present study, we have carried out detailed examination of the spectrum of the 1 : 1 complex by applying ultraviolet–ultraviolet (UV–UV) hole burning and rotational contour analysis. In what follows, we

briefly describe the experimental setup and present the LIF and hole burning spectra. Then we discuss the internal rotation of ammonia in the complex to explain the observed spectra. First, symmetry arguments and the correlation between free and hindered rotation of ammonia are discussed, then a Hamiltonian appropriate to the internal rotation–rotation problem in the "molecule on a plane" system is derived. Simulation of the observed rotational contour is performed with the model Hamiltonian to extract several spectroscopic parameters, and the structure and the anisotropy of the intermolecular potential are discussed on the basis of the results. Finally, vibronic bands of vdW modes appearing in the hole burning spectra are described to show the substantial contribution of vdW motions other than the internal rotation.

Experimental

Details of the experimental setup for LIF and UV–UV hole burning measurements have been presented elsewhere.[20,21] Anthracene–(ammonia)$_n$ were generated in a supersonic expansion from a pulsed solenoid valve (General Valve, Series 9) with a 0.8 mm diameter orifice operating at 10 Hz. The solid sample of anthracene was placed in a small holder (heated to ~120 °C) attached to the valve. The sample vapors were entrained in helium carrier gas premixed with 0.3–1.0% of NH_3 (or ND_3), and pulsed out into the vacuum chamber (~10 mPa in operation) at a stagnation pressure of 0.2–0.4 MPa. Anthracene and ammonia were used at commercially available purities.

LIF spectra of anthracene–(ammonia)$_n$ were observed at 355–375 nm using a XeCl excimer-laser pumped dye laser (Lambda Physik LPX100/LPD3000 or COMPex 102/SCANmate 2E with DMQ dye). The UV light crossed the free jet 10–15 mm downstream of the nozzle. Fluorescence was detected by a photomultiplier, whose output was averaged with a boxcar and stored into a personal computer. The laser wavelength was calibrated with Ne optogalvanic signals. The bandwidth of the UV light was 0.02 or 0.12 cm^{-1} with or without an intracavity etalon, respectively. The laser power was kept low so as to avoid saturation especially in etalon scans. For hole burning measurements, two laser pulses of similar wavelengths were employed with the temporal separation of ~200 ns. The first laser (denoted as *burn*) was scanned, while the second laser (denoted as *probe*) was fixed to the electronic origin. Depletion in the ground state population by the *burn* pulse was monitored as a decrease in fluorescence by the *probe* pulse. To induce a large population hole, strong *burn* pulses (up to several mJ pulse^{-1}) from the excimer laser pumped dye laser (LPX100/LPD3000) were mildly focused, while the doubled output (well below 0.1 mJ pulse^{-1}) of a dye laser (LAS, LDL205 with LDS 750) pumped by a Nd^{+}:YAG laser (Spectra Physics, GCR-4) was used as *probe* after collimation with an aperture of 2–3 mm in diameter.

Results

Fig. 1 shows the LIF spectrum of the anthracene–(NH$_3$)$_n$ clusters in the region of 361–367 nm. The large peak at 361.08 nm (27 695 cm^{-1}) has been assigned to the origin of the S_1–S_0 electronic transition for the anthracene monomer.[22] Small sharp peaks appearing to the red of the monomer origin were absent when using pure anthracene–He expansions, so they were certainly due to anthracene–(NH$_3$)$_n$. Among them, the least red-shifted band at 362.2 nm exhibiting a closely spaced (~2 cm^{-1}) doublet was assigned to the electronic origin of anthracene–NH_3 because it was dominant when the NH_3 concentration or the stagnation pressure is low. (This assignment was confirmed by the hole burning and rotational contour measurements as described in the later sections.) No peaks assignable to vibronic bands of the complex were evident in the LIF spectrum. Other bands of higher clusters were also subjected to the hole burning measurements (spectra not shown), to sort out the peaks belonging to the same spectral carriers. From the results and the examination of the concentration and pressure dependences, their size assignments were tentatively made as indicated in Fig. 1.

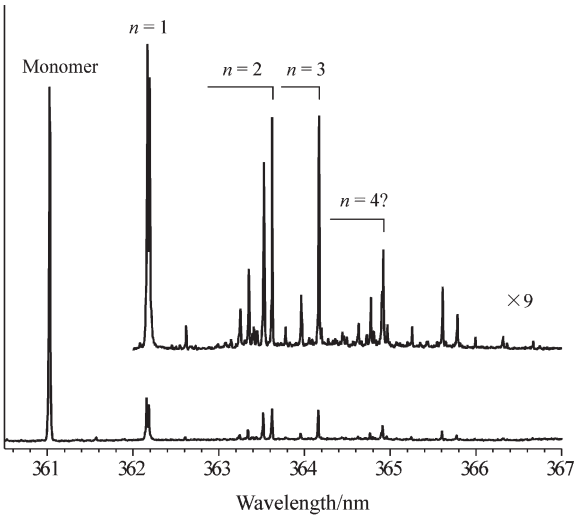

Fig. 1 LIF spectrum of the anthracene–(NH$_3$)$_n$ clusters in the monomer origin region.

The close up of the origin band of anthracene–NH_3 recorded with higher resolution is shown in Fig. 2. The two peaks at ~27 605.5 and ~27 607.5 cm^{-1} show almost similar intensities, regardless of the cooling conditions in supersonic expansions (*e.g.*, the nozzle–probed region distance and the stagnation pressure). Their rotational fine structures are quite different from each other, as discussed later. On the other hand, the small hump at ~27 604 cm^{-1} grew in intensity in warmer conditions, and thus it should be a hot band transition of the complex. It is noted that the small band at ~27 609 cm^{-1} has been assigned to anthracene–H_2O,[18] probably produced

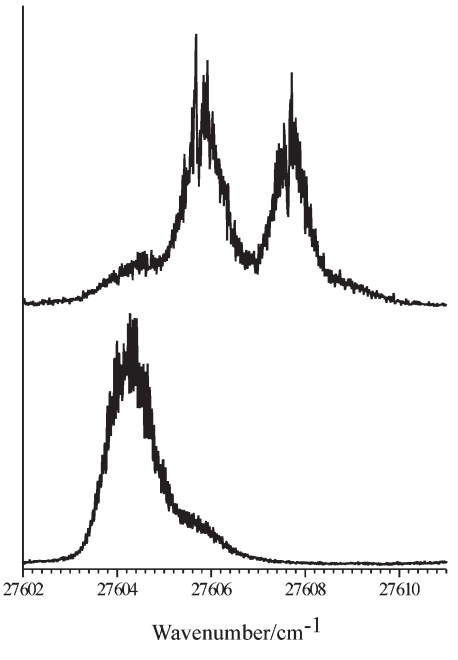

Fig. 2 Close up of the origin bands of anthracene–NH_3 (upper trace) and anthracene–ND_3 (lower trace).

from water residing in the sample handling system. The corresponding region of anthracene–ND_3 is also shown in Fig. 2. The doublet peaks collapse into a single band at ~27 604 cm^{-1} by the substitution from NH_3 to ND_3. A small shoulder at ~27 605.5 cm^{-1} seems to be due to complex(es) with partially deuterated ammonia (mostly NHD_2) formed *via* D/H exchange reaction with contaminating water.

Hole burning spectra were observed by fixing the *probe* laser to each of the two peaks of the anthracene–NH_3 origin band, as shown in Fig. 3. The spectrum with probing the upper peak (denoted as band A) shows no signal at the position of the lower peak (denoted as band B), and *vice versa*. This fact indicates that the spectral carriers of the two peaks are different from one another. Because the spectra were recorded with a strong *burn* laser, the origin bands suffer from saturation broadening but bands indiscernible in the LIF spectrum show up clearly. The spectra exhibit a number of vibronic bands with irregular spacing in the low energy region (<100 cm^{-1} above the origins). The vibronic activities, probed with the peaks A and B, are very different from each other: there is no match up of excitation energies between the bands observed in the spectra shown in Fig. 3, except for those within ~20 cm^{-1} above the origins.

Analysis

The S_1–S_0 origin band of anthracene–NH_3 shows the characteristic doublet feature. As for the closely related benzene–water[14] and –ammonia,[9] one of the doublet components is assigned to the transition from the first excited state of internal rotation of ammonia, and the other to that from the ground state. This assignment is qualitatively rationalized as follows. First, the two internal states are associated with the different [*ortho* ($I = 3/2$) and *para* ($I = 1/2$)] nuclear spin states of ammonia hydrogens (as described in detail later) and thus the first excited state cannot be relaxed to the ground state because of extremely slow nuclear spin conversion in supersonic expansions.[23] The populations of the two states are unchanged in the adiabatically cooled complex, which is in accord with the experimental observation that the relative intensities of the doublet peaks are essentially constant against the cooling conditions. Second, the splitting between the doublet peaks is the difference between the excitation energies of the first excited state from the ground state in the S_1 and S_0 manifolds. Since the interval between the two internal states is essentially a tunneling splitting due to the libration of ammonia, it reduces significantly by the isotopic substitution from NH_3 to ND_3, resulting in much smaller splitting in the excitation spectrum as actually observed. Third, the *ortho* and *para* states in the complex correlate, respectively, to the rotational states with $k = 3n$ and $k \neq 3n$ of ammonia in the free rotation limit, where k is the projection of the rotational angular momentum onto the ammonia C_3 axis and n is an integer.[24] Thus, it is expected that the intermolecular vibrational energy structures are quite different from one another for the two nuclear spin states when the libration of ammonia is extensive. This explains the notably different vdW activities in the hole burning spectra recorded by probing the two different splitting components. In the following sections, the assignment of the doublet peaks to the two internal rotation states is confirmed by symmetry arguments and an analysis of the coupling between the internal and end-over-end rotations.

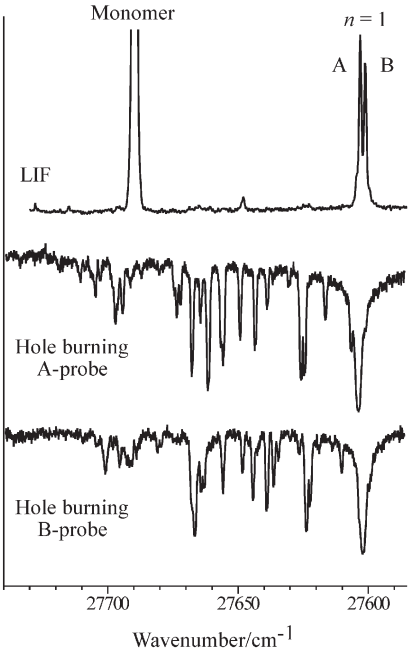

Fig. 3 LIF and UV–UV hole burning spectra of anthracene–NH_3.

1 Symmetry group consideration

For nonrigid systems, such as anthracene–ammonia with nearly free internal rotation of ammonia, symmetry classification of energy levels and optical selection rules should be based on the molecular symmetry (MS) group.[25] In the present study, we do not include the following two internal motions of anthracene–ammonia in the symmetry consideration: (1) the movement of ammonia from one side of the aromatic ring to the other and (2) the umbrella inversion of ammonia. The exclusion of the first motion is valid since the heavy ammonia molecule cannot move through such a long distance. The tunneling splitting caused by the second motion is less than 1 cm^{-1} in the case of free NH_3,[26] and it is expected to become smaller on formation of the hydrogen bond in the complex. In addition, the excitation spectrum will only show the difference between the tunneling splittings in the S_1 and S_0 manifolds. It has been found that such a splitting is too small to be observed in the present experiments as expected. This validates the second assumption.

The complex fixed (X, Y, Z) axes and the ammonia fixed (x, y, z) axes are defined as shown in Fig. 4, and the three Euler angles, θ, φ, and χ, between the two axis systems are given with the commonly used convention (for example see ref. 27) By using the coordinate systems thus defined, the translation of the ammonia center of mass is expressed with the (X, Y, Z)

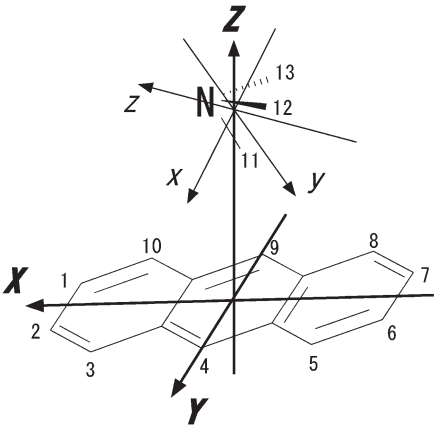

Fig. 4 Complex and ammonia fixed coordinate systems and hydrogen atom numbering in anthracene–NH_3.

coordinate of the origin of the (x, y, z) system, and the internal rotation of ammonia with the Euler angles. We hereafter denote the translational motions as "vdW vibrations" to distinguish them from the internal rotation.

The MS group consists of permutations of identical nuclei, inversion of spatial coordinates, and their products, which make feasible transformation of the molecule. With the operational definition of feasibility, there are 12 allowed operations for the anthracene–ammonia system, and thus the appropriate MS group is designated as G_{12}. The character table of the group is presented as Table 1. Here the symmetry operations are expressed by the permutations of 13 hydrogen nuclei in the complex, of which numbering is shown in Fig. 4 (the associated permutations of carbon nuclei are omitted for simplicity). Transformation properties of the internal coordinates are also listed in the table. It is noted that the MS group is isomorphic to the C_{6v} and D_{3h} point groups. Below, the four nondegenerate irreducible representations (A_1, A_2, B_1, and B_2) are expressed as $\Gamma_{A/B}$, while the two double degenerate ones (E_1 and E_2) are expressed as Γ_E.

The total wavefunction of the anthracene–ammonia complex is given in the zeroth order approximation that ignores the coupling between different internal degrees of freedom:

$$\psi_{total} = \psi_{vibronic}\psi_{vdW}\psi_{introt}\psi_{rot}\psi_{nspin} \quad (1)$$

where ψ's in the right hand side are the anthracene's vibronic, vdW vibrational, internal rotation, over-all rotation, and nuclear spin wavefunctions, respectively. We deal with the origin band of the S_1–S_0 electronic transition, and the symmetry of $\psi_{vibronic}$ so concerned is that of the electronic wavefunction of free anthracene: B_2 for S_1 and A_1 for S_0. For ψ_{vdw}, the first excited states of the X-, Y-, and Z-translational motions belong to B_1, B_2, and A_1, respectively. The over-all rotation wavefunction is that of an asymmetric top molecule, $\psi_{rot} = |J,K_X,K_Y\rangle$, where K_X and K_Y are the the projection of the total angular momentum J to the X and Y axes, respectively. The symmetry of ψ_{rot} changes as K_X and K_Y are even or odd, as listed in Table 2. It is noted that ψ_{rot} always belongs to $\Gamma_{A/B}$. Because the total wavefunction should be (anti-) symmetric to even (odd) permutations of fermions, it belongs to the irreducible representation, B_1 or B_2, in MS group G_{12}. Then, the aforementioned arguments showing $\psi_{vibronic}$, ψ_{vdw}, and $\psi_{rot} \in \Gamma_{A/B}$ leads to the following conclusion: both ψ_{introt} and ψ_{nspin} should belong to the same symmetry, $\Gamma_{A/B}$ or Γ_E.

Anthracene–NH_3 has $2^{13} = 8192$ reducible nuclear spin wavefunctions as it contains 13 hydrogen atoms. They are reduced into $A_1 : A_2 : B_1 : B_2 : E_1 : E_2 = 1152 : 960 : 960 : 1024 : 992 : 1056 = 36 : 30 : 30 : 32 : 31 : 33$ irreducible representations. This leads to the nuclear-spin statistical weights of $\Gamma_{A/B} : \Gamma_E = 2 : 1$, which are the same for the free *ortho* and *para* NH_3 molecules. In the case of anthracene–ND_3, $A_1 : A_2 : B_1 : B_2 : E_1 : E_2 = 195 : 168 : 166 : 175 : 248 : 264$, and thus the nuclear-spin statistical weights are $\Gamma_{A/B} : \Gamma_E = 11 : 8$, which match with free ND_3.

The internal rotation wavefunction ψ_{introt} is expressed as a linear combination of symmetric top wavefunctions that represent free rotation of ammonia, $|j,k,m\rangle$, where j is the internal rotation angular momentum with k and m being its projections to the z and Z axes, respectively. Irreducible representations of $|j,k,m\rangle$ are summarized in Table 3. It is noted that wavefunctions with $k = 3n$ belong to $\Gamma_{A/B}$ and are coupled with *ortho* nuclear-spin states, while those with $k \neq 3n$ to Γ_E with *para* nuclear spins. The density of states for Γ_E wavefunctions is twice of that for $\Gamma_{A/B}$ because the former correlates to $k = \pm1, \pm2, \pm4, \pm5,...$ while the latter to $k = 0, \pm3, \pm6,...$ In the case of adiabatically cooled supersonic expansions, almost all the molecules relax to the lowest internal rotation states whilst preserving their nuclear spin wavefunctions. Thus, the relative populations of the lowest states belonging to $\Gamma_{A/B}$ and Γ_E are 1 : 1 for anthracene–NH_3 with the statistical weights of $\Gamma_{A/B}$ (*ortho*) : Γ_E (*para*) = 2 : 1. This conclusion agrees well with almost the same intensities for the observed bands A and B. The relative populations for Anthracene–ND_3 are 11 : 16 for $\Gamma_{A/B}$ and Γ_E.

Next we briefly discuss the selection rules for electric transitions between the S_1 and S_0 manifolds. The electric transition moment in the anthracene moiety is of B_2 symmetry and thus provides Y-polarized transitions, for which symmetries of $\psi_{vdw}\psi_{introt}$ in the upper and lower states should be the same. The X- and Z-polarized transitions are vibronically allowed by the coupling of S_1 with other electronic states through intermolecular modes. In the fluorescence excitation spectrum, only the transitions diagonal to the vdW vibrations and internal rotation appeared, indicating similar cluster geometries in S_1 and S_0 and ineffective vibronic coupling. The transitions identified in the hole burning spectra are assigned to those to higher $\psi_{vdw}\psi_{introt}$ excited states in S_1, which gain some intensity either by small Franck–Condon overlap or by small vibronic activities.

Table 1 Character table of group G_{12} appropriate to anthracene–NH_3

	P_{even}	P_{odd}	P_{even}	P_{odd}	P_{even}*	P_{odd}*
Symmetry operation	E	(16)(27)(38)(49)(5 10)	(11 13 12) (11 12 13)	(16)(27)(38)(49) (5 10)(11 13 12) (16)(27)(38)(49) (5 10)(11 12 13)	(12)(3 10)(49)(58) (67)(12 13)* (12)(3 10)(49)(58) (67)(11 13)* (12)(3 10)(49)(58) (67)(11 12)*	(17)(26)(35)(8 10) (12 13)* (17)(26)(35)(8 10) (11 13)* (17)(26)(35)(8 10) (11 12)*
Equivalent operation	(X, Y, Z)	$(-X, -Y, Z)$	(X, Y, Z)	$(-X, -Y, Z)$	$(X, -Y, Z)$	$(-X, Y, Z)$
	R_Z^0 θ φ χ	R_Z^π θ $\varphi - \pi$ χ	R_Z^0 θ φ $\chi \pm 2\pi/3$	R_Z^π θ $\varphi - \pi$ $\chi \pm 2\pi/3$	R_Y^π θ $\varphi - \pi$ $-\chi, -\chi \pm 2\pi/3$	R_X^π θ $\varphi - \pi$ $-\chi, -\chi \pm 2\pi/3$
A_1	1	1	1	1	1	1
A_2	1	1	1	1	−1	−1
B_1	1	−1	1	−1	1	−1
B_2	1	−1	1	−1	−1	1
E_1	2	−2	−1	1	0	0
E_2	2	2	−1	−1	0	0

Table 2 Symmetry of over-all rotational function: $|J,K_X,K_Y\rangle$

K_X, K_Y	Symmetry
Even, even	A_1
Even, odd	B_2
Odd, even	A_2
Odd, odd	B_1

2 Model for internal rotation

In this section we derive the correlation between the rotation of free ammonia and (hindered) internal rotation in the complex by using a simple model. Here the following two approximations are invoked: (1) ammonia is located above the centre of the aromatic plane, and (2) the vdW vibrations are of much smaller amplitude than the internal rotation and they are decoupled from one another. The first approximation is verified later by the rotational contour analysis. The second approximation is seriously challenged when considering the exact energy levels for intermolecular motions as discussed in the subsequent section, but it is valid enough for discussing the energy level pattern of the internal rotation and its effects on rotational fine structure. Then, the Hamiltonian appropriate to the internal rotation is

$$H_{\text{introt}} = b\boldsymbol{j}^2 + (c-b)j_z^2 + V(\phi,\theta,\chi) \tag{2}$$

with $\boldsymbol{j}$ being the angular momentum of rotating ammonia, b and c its rotational constants, and $V(\phi,\theta,\chi)$ the potential for the internal rotation. The potential should satisfy,

$$\begin{aligned} V(\phi,\theta,\chi) &= V(-\phi,\theta,-\chi) = V(\phi,\theta,\chi \pm 3\pi/2) \\ &= V(\phi \pm \pi,\theta,\chi) \end{aligned} \tag{3}$$

because of the symmetry of the system. With the symmetry requirements, the potential is expanded with the rotation matrices, $D^j_{m,k}(\phi,\theta,\chi)$, that span a complete set for an arbitrary function of three dimensional rotation as

$$\begin{aligned} V(\phi,\theta,\chi) = \sum_{j,l,n} V^j_{2l,3n}[&D^j_{2l,3n}(\phi,\theta,\chi) \\ &+ (1-\delta_{n^2+l^2,0})(-1)^n D^j_{-21,-3n}(\phi,\theta,\chi)] \end{aligned} \tag{4}$$

with j and $n = 0, 1, 2, \cdots$, $l = 0, \pm1, \pm2, \cdots$, and $V^j_{m,k}$ being expansion coefficients.

To reveal correlations between the energy level structure of the internal rotation and the global features of $V(\phi,\theta,\chi)$ with minimal parameterization, we include only the dominant terms, $D^1_{0,0}$, $D^2_{0,0}$, $D^2_{\pm2,0}$, and $D^3_{0,\pm3}$, in the expansion of eqn. (4), to have

$$\begin{aligned} V(\phi,\theta,\chi) = V^1_{0,0}\cos\theta + \frac{1}{2}V^2_{2,0}(3\cos^2\theta - 1) \\ + \sqrt{\frac{3}{2}}V^2_{2,0}\cos 2\phi \sin^2\theta + \frac{\sqrt{5}}{2}V^3_{0,3}\sin^3\theta\cos 3\chi \end{aligned} \tag{5}$$

Table 3 Irreducible representations of internal rotation function

Wavefunction		Symmetry
$k = 3n$;		
$\psi_{\text{introt}} = \dfrac{\lvert j,k,m\rangle + (-1)^{k+m+s}\lvert j.,-k,-m\rangle}{\sqrt{2}}$	m = even, s = 0	A_1
	m = even, s = 1	A_2
	m = odd, s = 0	B_1
	m = odd, s = 1	B_2
$k \neq 3n$;		
$\psi_{\text{introt}} = \begin{pmatrix} \lvert j,k,m\rangle \\ \lvert j,-k,-m\rangle \end{pmatrix}$	m = even	E_2
	m = odd	E_1

Eigenvalues and corresponding wavefunctions are obtained by diagonalization of the Hamiltonian matrices constructed upon the symmetry-adopted basis functions listed in Table 3. We examine various sets of the potential parameters, and an example of calculated energy levels is indicated in Fig. 5. The parameters used are estimated from the results of the *ab initio* calculation on benzene–ammonia,[9] while the monomer rotational constants are taken from refs. 28 and 29. The figure demonstrates that potential anisotropy makes free-rotor states, having $(2j+1)$-fold degeneracy in m, split into levels with different symmetries. The lowest *ortho* state is always of A_1 symmetry, which is correlated to the free rotor state with $(j, k) = (0, 0)$. The lowest *para* state is of E_1 or E_2 symmetry, depending on the potential parameters, both of which are correlated to $(j, k) = (1, \pm1)$. It is confirmed that isotopic substitution from NH_3 to ND_3 reduces the interval between the lowest *ortho* and *para* states by far more than 1/2 with moderate potential anisotropy.

3 Effective rotational Hamiltonian

When the complex exhibits internal rotation as in the present case of anthracene–ammonia, the internal and end-over-end rotational angular momenta, $\boldsymbol{j}$ and $\boldsymbol{l}$, are vectorically coupled to make the total angular momentum: $\boldsymbol{J} = \boldsymbol{j} + \boldsymbol{l}$. The Hamiltonian to consider in the internal rotation–rotation problem is

$$H = H_{\text{introt}} + H_{\text{frame}} \tag{6}$$

where the Hamiltonian for the end-over-end rotation is given with the rotational constants of the complex, A, B and C, as

$$\begin{aligned} H_{\text{frame}} &= Al_X^2 + Bl_Y^2 + Cl_Z^2 \\ &= \frac{A+B}{2}(\boldsymbol{J}-\boldsymbol{j})^2 + \frac{2C-A-B}{2}(J_Z - j_Z)^2 \\ &\quad + \frac{A-B}{4}\left[(J_+ - j_+)^2 + (J_- - j_-)^2\right] \\ &= \frac{A+B}{2}\boldsymbol{J}^2 + \frac{2C-A-B}{2}J_Z^2 + \frac{A-B}{4}(J_+^2 + J_-^2) \\ &\quad + \frac{A+B}{2}\boldsymbol{j}^2 + \frac{2C-A-B}{2}j_Z^2 + \frac{A-B}{4}(j_+^2 + j_-^2) \\ &\quad - 2CJ_Z j_Z - \frac{A+B}{2}(J_+ j_- + J_- j_+) \\ &\quad - \frac{A-B}{2}(J_+ j_+ + J_- j_-) \end{aligned} \tag{7}$$

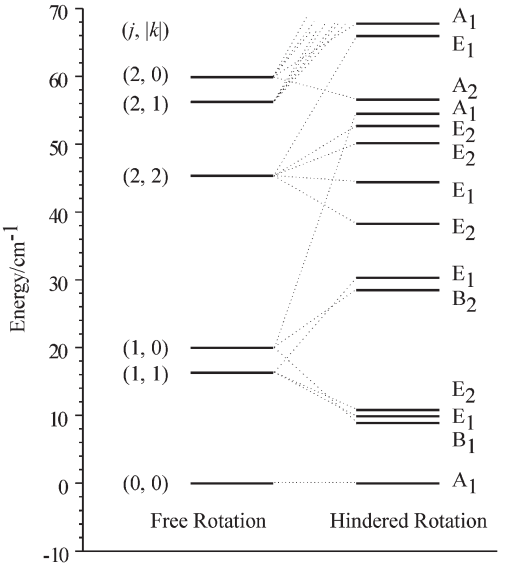

Fig. 5 Correlation diagram for internal rotation in anthracene–NH_3. For hindered rotation, potential parameters used are: $V^1_{0,0} = -100$ cm^{-1}, $V^2_{0,0} = 100$ cm^{-1}, and $V^2_{2,0} = V^2_{0,3} = -20$ cm^{-1}. Energies indicated are values relative to the lowest states.

The terms in the first line of the last equation, solely containing total angular momentum, are hereafter denoted as $H^{(0)}_{\rm frame}$. The second line depends on the internal rotation angular momentum only, and it is included into $H_{\rm introt}$. Since A, B and C are three orders of magnitude smaller than b and c, effects of the inclusion are negligible. The rest terms representing the coupling between the internal rotation and over-all rotation are denoted as $H'_{\rm frame}$.

By solving the eigenvalue problem on $H_{\rm introt}$ as described in the preceding section, the wavefunctions $|\psi^{(i)}_{\rm introt}\rangle$ and their energy E_i's are obtained. The Hamiltonian matrix of $H_{\rm introt}+H^{(0)}_{\rm frame}$ becomes block diagonal in terms of $|\psi^{(i)}_{\rm introt}\rangle$ when using $|\psi^{(i)}_{\rm introt}\rangle|J,K,M\rangle$ as the basis set, while the matrix elements of $H_{\rm frame}$ remain off-diagonal. An exact calculation of the energy levels requires diagonalization of Hamiltonian matrices constructed with the basis functions spanning i, J and K, which will be a demanding computation since large values of J (up to $\sim$50) must be included to simulate the observed spectrum of anthracene–ammonia.

To overcome the difficulty, we apply the Van Vleck transformation that unitary transforms Hamiltonian so as to become block diagonal by a perturbative transfer of off-diagonal matrix elements among different blocks into the diagonal blocks.[30,31] This transformation is valid since energies of over-all rotation are much smaller than intervals between the E_i's (in the order of b and c) in the complex. The effective Hamiltonian from first-order perturbation theory is given as

$$\begin{aligned} H^{(1)\,eff}_{\rm frame} &\equiv \left\langle \psi^{(i)}_{\rm itnrot}\middle| H'_{\rm frame}\middle|\psi^{(i)}_{\rm introt}\right\rangle \\ &= -2C\left\langle \psi^{(i)}_{\rm itnrot}\middle| j_Z\middle|\psi^{(i)}_{\rm itnrot}\right\rangle J_Z \\ &\quad -\frac{A+B}{2}\left[\left\langle \psi^{(i)}_{\rm itnrot}\middle| j_-\middle|\psi^{(i)}_{\rm itnrot}\right\rangle J_+ \right. \\ &\quad \left. +\left\langle \psi^{(i)}_{\rm itnrot}\middle| J_+\middle|\psi^{(i)}_{\rm itnrot}\right\rangle J_-\right] \\ &\quad -\frac{A-B}{2}\left[\left\langle \psi^{(i)}_{\rm itnrot}\middle| j_+\middle|\psi^{(i)}_{\rm itnrot}\right\rangle J_+ \right. \\ &\quad \left. +\left\langle \psi^{(i)}_{\rm itnrot}\middle| j_-\middle|\psi^{(i)}_{\rm itnrot}\right\rangle J_-\right] \end{aligned} \tag{8}$$

Here we recall that $|\psi^{(i)}_{\rm introt}\rangle$ is expanded as a linear combination of free rotor basis functions:

$$\left|\psi^{(i)}_{\rm inrot}\right\rangle = \sum_{j,k,m} C^{(i)}_{j,k,m}|j,k,m\rangle \tag{9}$$

with $C^{(i)}_{j,k,m}$ being an expansion coefficient. Then the matrix elements on j are evaluated as

$$\left\langle \psi^{(i)}_{\rm inrot}\middle| j_Z\middle|\psi^{(i)}_{\rm inrot}\right\rangle = \sum_{j,k,m} m\left|C^{(i)}_{j,k,m}\right|^2 \equiv p \tag{10}$$

$$\begin{aligned} \left\langle \psi^{(i)}_{\rm inrot}\middle| j_\pm\middle|\psi^{(i)}_{\rm inrot}\right\rangle &= \sum_{j,k,m}\sqrt{j(j-1)-m(m\pm1)} \\ &\quad \times C^{(i)}_{j,k,m\pm1}C^{(i)}_{j,k,m} = 0 \end{aligned} \tag{11}$$

The last equation holds because $|\psi^{(i)}_{\rm introt}\rangle$ includes $|j,k,m\rangle$ with either odd or even m only. We finally have the following first-order correction for over-all rotation:

$$H^{(1)eff}_{\rm frame} = -2CpJ_Z \tag{12}$$

Eqn. (10) shows that the parameter p is the projection of internal rotation angular momentum onto the Z axis. It vanishes for all the $\Gamma_{A/B}$ (*ortho*) internal rotation states, as is evident from the functional form of their irreducible basis functions with $k = 3n$ listed in Table 3. On the other hand, Γ_E (*para*) states have non-zero value of p. It is noted that the doubly degenerate wavefunctions for Γ_E are composed of functions with either $k = 3n+1$ or $-(3n+1)$ and that p for the two states have the same absolute values but opposite signs. Thus an irreducible set, $|j,3n+1,m\rangle|J,K,M\rangle$ and $|j,-(3n+1),m\rangle|J,-K,M\rangle$, are used as the internal rotation–rotation basis set for Γ_E states.

In the first-order treatment, the internal rotation produces no modification of rotational energy levels in $\Gamma_{A/B}$ states. This is because the internal rotation angular momentum in the states has no orientation along the Z axis. Consequently, transitions for $\Gamma_{A/B}$ states exhibit a spectrum that is identical to an ordinary rigid asymmetric top molecule. For Γ_E states, the p parameter depends on $V(\phi,\theta,\chi)$. When the potential is expanded as eqn. (5), $D^1_{0,0}$ only brings the Z-axis orientation and thus p always vanishes for $V^1_{0,0} = 0$. When $V^2_{2,0} = 0$ with $V^1_{0,0} \neq 0$, the rotation around the Z axis is preserved and $|p| = 1$ or 0 for the lowest E_1 or E_2 state, respectively. As $|V^2_{2,0}|$ becomes larger, $|p|$ for E_1 is reduced monotonically while that for E_2 first increases to its maximum and then falls down. Both approach zero as the Z-axis rotation is completely hindered with infinite $|V^2_{2,0}|$.

Results from a model calculation are indicated in Fig. 6. The actual value of $|p|$ certainly depends on the other potential parameters, but the general trend of its dependence on $|V^2_{2,0}|$ is essentially unaffected. We note that the second-order contributions of $H'_{\rm frame}$ are effectively included as slight modifications of the rotational constants, A, B and C. The changes are estimated to be too small to be detected in the present experimental results.

4 Rotational contour analysis

The rotational contours of the observed doublet bands of anthracene–NH_3 are analyzed by adopting the effective rotational Hamiltonian derived in the preceding section. First we assign the band of the lowest internal rotation state with $\Gamma_{A/B}$ symmetry among the two. The rotational contour for the $\Gamma_{A/B}$ band has been simulated for several centre-of-mass distances in an appropriate range (R = 3.4–3.8 Å). Here the rotational constants of the complex are calculated with the monomer constants from ref. 32 by regarding the NH_3 molecule as a point mass on the anthracene plane. This simplification is adopted because the present spectral resolution is insufficient to discuss in detail about the geometry, *e.g.*, averaged orientation of ammonia relative to the aromatic ring. In addition, the simulated spectra are not so sensitive to the displacements of ammonia parallel to the aromatic plane. Thus it is assumed that NH_3 is located above the centre of anthracene, on the basis of the previous empirical model calculation

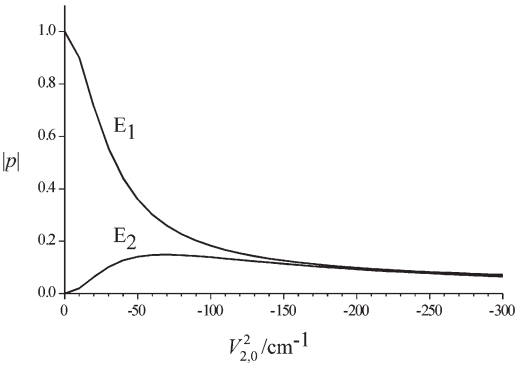

Fig. 6 Dependence of the coupling parameter, p, on $V^2_{2,0}$. Other potential parameters fixed as: $V^1_{0,0} = -100$ cm^{-1}, $V^2_{0,0} = 100$ cm^{-1}, and $V^2_{0,3} = -20$ cm^{-1}.

that showed this position of ammonia corresponded to the global minimum geometry.[19] Rotational temperature and spectral line width are set to the values ($T_R = 3$ K and $\Delta\nu = 0.02$ cm^{-1}) from the results of the monomer 0_0^0 band recorded under identical experimental conditions. Comparison between the observed and simulated spectra shows that the rotational contour of the band A is well reproduced with $R = 3.6$ Å, as indicated in Fig. 7. The uncertainty for R is estimated to be less than 0.1 Å. In the present analysis, the centre-of-mass distances in the upper and lower states are set to be the same. The difference should be also less than 0.1 Å, judging from the good match of the simulated contour to the observed one. More importantly, the agreement confirms the assignment of the higher peak A to the transition in the $\Gamma_{A/B}$ (*ortho*) state.

Next we analyze the band B, which should be due to the lowest Γ_E (*para*) internal rotation state. Examination of various sets of the parameters, p' and p'' (p for the upper and lower states, respectively) ranging from 0 to 1, with R fixed to 3.6 Å has revealed that observed rotational contour of this band is reproduced well either when $p' = 0.0$ and $p'' = 0.2$ or $p' = 0.4$ and $p'' = 0.6$. The uncertainties for p's are less than 0.1. Qualities of the agreements are essentially the same for the two sets, so we need further discussion on the derived parameters to differentiate the two possibilities.

First, we assume the band B as the transition due to the lowest E_2 internal rotation state. The difference between p' and p'' becomes ~0.2 only when $|V_{2,0}^2(S_0)| > |V_{2,0}^2(S_1)| \approx 0$ or $|V_{2,0}^2(S_0)| \ll |V_{2,0}^2(S_1)|$, as Fig. 6 shows. The former condition is implausible since the red shift of the Γ_E band from the $\Gamma_{A/B}$ band implies the higher potential anisotropy in S_1, which will give the larger $|V_{2,0}^2|$. The latter condition would involve a drastic change of the internal rotation potential by the S_1–S_0 electronic excitation, but this is unlikely judging from the fact that there is almost no vdW activities in the electronic transition. These arguments stand against the possibility for the assignment of the band B to the lowest E_2 state.

Then we consider the other choice that the band B is due to the lowest E_1 state. For $p' = 0.0$ and $p'' = 0.2$, the potential parameters should meet the implausible condition: $|V_{2,0}^2(S_0)| \ll |V_{2,0}^2(S_1)|$. On the other hand, the set of $p' = 0.4$ and $p'' = 0.6$ is realized when $|V_{2,0}^2(S_0)| < |V_{2,0}^2(S_1)|$, which is consistent with the frequency ordering of the $\Gamma_{A/B}$ and Γ_E bands. The change of the $V_{2,0}^2$ parameter by the electronic excitation seems to be reasonable, according to the model calculation represented in Fig. 6. Thus, the band B is assigned most probably to the transition associating with the lowest E_1 internal rotation state, for which the p parameters are determined to be 0.4 and 0.6 in the S_1 and S_0 manifold, respectively. The simulated spectrum for the parameters is also indicated in Fig. 7.

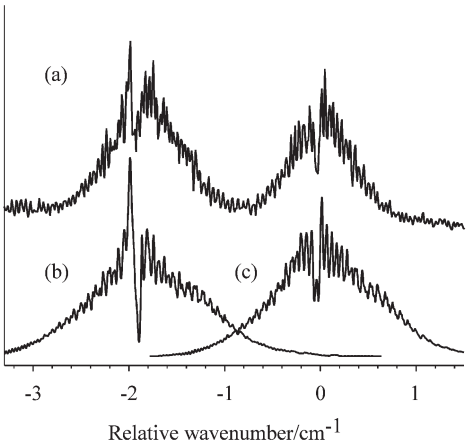

Fig. 7 Observed [(a)] and simulated [(b) and (c)] spectra of the origin band of anthracene–NH_3. Trace (b) is calculated as the Γ_E state with $p' = 0.4$ and $p'' = 0.6$, while trace (c) as the $\Gamma_{A/B}$ state. In both cases, the centre-of-mass distance is fixed as $R = 3.6$ Å.

We find that the rotational contour of the origin band of anthracene–ND_3 cannot be reproduced either as a transition in $\Gamma_{A/B}$ or in Γ_E. The spectrum looks too congested to show any (partially) resolved rotational fine structure. This confirms that the band is actually composed of two overlapping transitions, *i.e.*, those due to the ground and the first excited internal rotation states. The splitting between them is well below ~0.5 cm^{-1}. It is noted that the value for anthracene–NH_3 is ~2 cm^{-1}.

Discussion

The present study on anthracene–ammonia has confirmed that the attached ammonia lies above the centre of the middle aromatic ring of anthracene. The centre-of-mass distance between anthracene and ammonia is determined to be 3.6 Å, which is close to those in the related complexes composed with an aromatic molecule and a proton donor: benzene–HF (3.14 Å in S_0),[3] benzene–HCl (3.59 and 3.64 Å in S_0 and S_1, respectively),[4,5,33] benzene–H_2O (3.33 and 3.32 Å in S_0 and S_1),[6,7,14] and benzene–NH_3 (3.56 Å in S_0).[9] In these complexes, at least two different isotopomers of the proton donor have been examined to show that their X–H bonds (X = F, Cl, O, or N) point toward the aromatic plane in the vibrationally averaged structures over zero-point motions. The similarity in the centre-of-mass distances corroborates that anthracene–ammonia is also classified as a typical π hydrogen bonded aromatic complex, though we lack experimental information on the orientation of ammonia at the moment. It is shown that the change in the distance by the S_1–S_0 electronic excitation is marginal in anthracene–ammonia, which is in accord with related π hydrogen bonded complexes.

In the present study, the rotational contour in the internal rotation excited state has been successfully analyzed with the effective Hamiltonian including the coupling between the internal and end-over-end rotations. So far, there have been scarce reports on such an angular momentum coupling appearing in the electronic excitation spectra of aromatics complexed with a molecule above their planes.[14,34,35] In anthracene–ammonia, the coupling constant, p, representing the projection of the internal rotation angular momentum onto the Z axis, is less than unity, that is expected for free rotation around the axis. This partial quench of the internal rotation is caused by the finite potential anisotropy, $|V_{2,0}^2|$, which originates from asymmetric π-electron distribution with respect to the long (X) and short (Y) axes of anthracene. Such an anisotropy has also been reported for aniline–N_2, the rotationally resolved excitation spectrum of which has been analyzed with a one-dimensional internal rotation model.[35] The derived potential barriers (25 and 60 cm^{-1} in S_0 and S_1) are much larger than the rotational constant of N_2 (2.0 cm^{-1}). This may not be the case for anthracene–ammonia, with which the internal rotation is only partially quenched. Aniline–N_2 shows a large increase in the anisotropy probably because of stronger binding and shorter intermolecular distance after electronic excitation. The trend is qualitatively in accord with anthracene–ammonia, in which p is quenched to a larger extent in S_1. In the case of benzene–water, the anisotropy is so small because of its high symmetry that the rotation around the Z axis is treated as essentially free.[7,8,14,15]

In the hole burning spectra recorded in this study, many of weak vibronic bands are observed in the low excess energy region (<100 cm^{-1} above the origins). They are assigned to transitions associated with the excitation of intermolecular vibrations, because anthracene possesses no such low-frequency modes.[36] The number of the observed bands is

much larger than that estimated for excited states of internal rotation with any form of the potential, $V(\phi,\theta,\chi)$. This shows that vdW vibrations involving the translation of the ammonia centre-of-mass contribute to some of the observed bands. If the internal rotation and the vdW vibrations are decoupled to one another, vibrational energies should be a sum of the independent terms corresponding to the two motions and the subsequent regularity in the level structre should be noticed. However, the observed hole burning spectra cannot be assigned on the basis of such a simple interpretation, implying substantial coupling between the internal rotation and the vdW vibrations. A similar extensive mixing among the intermolecular motions has been identified in benzene–water.[15,17,37,38] In particular, a full quantum treatment including all the degrees of freedom has been performed to analyze the intermolecular energy level structure.[17] The present observation on the rich spectral activities of the intermolecular modes makes anthracene–ammonia a particularly attractive system to apply such an extended analysis for evaluating the intermolecular potential with much improved accuracy.

Conclusion

In the present study, we report the S_1–S_0 excitation spectrum of the anthracene–ammonia complex to show details on internal rotation–rotation coupling in the π hydrogen bonded system. The NH_3 isotopomer of the complex has been found to exhibit a doublet origin, and we have confirmed that the two bands are assigned to the ground and the first excited states of the NH_3 internal rotation. To elucidate the observation, we derive the molecular symmetry group appropriate to the system, the energy level correlation of free and hindered rotation, and the model Hamiltonian describing the coupling between the internal and end-over-end rotations. Simulation of the observed rotational contour shows that ammonia is located on the centre of the aromatic plane with an intermolecular distance similar to the other π hydrogen bonded systems. The obtained effective coupling constant indicates the partial quenching of internal rotation angular momentum because of the potential anisotropy due to the different interaction along the long axis from that along the short axis of anthracene. Rich and irregular vibronic levels probed by the hole burning measurement are associated not only to the internal rotation but also to the translational motions of the ammonia centre-of-mass. For quantitative analysis of the data, fully coupled dynamics of the intermolecular vibrations should be considered.

Acknowledgements

The authors thank Prof. O. Kajimoto for his encouragement and support throughout the study. The present work has been partly supported by a Grant-in-Aid (No. 14340180) from the Ministry of Education, Science, Culture, and Sports of Japan. Financial supports from the Japan Atomic Energy Research Institute and the Sumitomo Science Foundation are also acknowledged.

References

1 G. C. Pimental, A. L. McClellan, *The Hydrogen Bond*, Freeman, San Francisco, CA, 1960.
2 G. A. Jeffrey, *An Introduction to Hydrogen Bonding*, Oxford University Press, Oxford, 1997.
3 F. A. Baiocchi, J. M. Williams and W. Klemperer, *J. Phys. Chem.*, 1983, **87**, 2079.
4 W. G. Read, E. J. Campbell, G. Henderson and W. H. Flygare, *J. Am. Chem. Soc.*, 1981, **103**, 7670.
5 W. G. Read, E. J. Campbell and G. Henderson, *J. Chem. Phys.*, 1983, **78**, 3501.
6 S. Suzuki, P. G. Green, R. E. Bumgarner, S. Dasgupta, W. A. Goddard III and G. A. Blake, *Science*, 1992, **257**, 942.
7 H. S. Gutowsky, T. Emilsson and E. Arunan, *J. Chem. Phys.*, 1993, **99**, 4883.
8 T. Emilsson, H. S. Gutowsky, G. de Oliveira and C. E. Dykstra, *J. Chem. Phys.*, 2000, **112**, 1287.
9 D. A. Rodham, S. Suzuki, R. D. Suenram, F. J. Lovas, S. Dasgupta, W. A. Goddard III and G. A. Blake, *Nature*, 1993, **362**, 735.
10 E. Arunan, T. Emilsson, H. S. Gutowsky, G. T. Fraser, G. de Oliveira and C. E. Dykstra, *J. Chem. Phys.*, 2002, **117**, 9766.
11 A. Courty, M. Mons, I. Dimicoli, F. Piuzzi, M.-P. Gaigeot, V. Brenner, P. de Pujo and P. Millié, *J. Phys. Chem. A*, 1998, **102**, 6590.
12 M. Mons, I. Dimicoli, B. Tardivel, F. Piuzzi, V. Brenner and P. Millié, *Phys. Chem. Chem. Phys.*, 2002, **4**, 571.
13 P. E. S. Wormer and A. van der Avoird, *Chem. Rev.*, 2000, **100**, 4109.
14 A. J. Gotch and T. S. Zwier, *J. Chem. Phys.*, 1992, **96**, 3388.
15 R. N. Pribble, A. W. Garrett, K. Haber and T. S. Zwier, *J. Chem. Phys.*, 1995, **103**, 531.
16 P. M. Maxton, M. W. Schaeffer and P. M. Felker, *Chem. Phys. Lett.*, 1995, **241**, 603.
17 W. Kim, D. Neuhauser, M. R. Wall and P. M. Felker, *J. Chem. Phys.*, 1999, **110**, 8461.
18 P. M. Palmer and M. R. Topp, *Chem. Phys.*, 1998, **239**, 65.
19 O. Anner and Y. Haas, *J. Phys. Chem.*, 1986, **90**, 4298.
20 M. Mitsui, Y. Ohshima, S. Ishiuchi, M. Sakai and M. Fujii, *Chem. Phys. Lett.*, 2000, **317**, 211.
21 M. Mitsui and Y. Ohshima, *J. Phys. Chem. A*, 2000, **104**, 8638.
22 W. R. Lambert, P. M. Felker, J. A. Sayge and A. H. Zewail, *J. Chem. Phys.*, 1984, **81**, 2195.
23 S. M. Beck, M. G. Liverman, D. L. Monts and R. E. Smalley, *J. Chem. Phys.*, 1979, **70**, 232.
24 C. H. Townes, A. L. Schawlow, *Microwave Spectroscopy*, Dover, New York, 1975.
25 P. R. Bunker, P. Jensen, *Molecular Symmetry and Spectroscopy*, NRC Press, Ottawa, 1998.
26 D. Papousek, J. M. R. Stone and V. Spirko, *J. Mol. Spectrosc.*, 1973, **48**, 17.
27 R. N. Zare, *Angular Momentum*, Wiley, New York, 1988.
28 P. R. Bunker, W. P. Kraemer and V. Spirko, *Can. J. Phys.*, 1984, **62**, 1801.
29 L. Fusina, B. DiLonardo and J. W. C. Johns, *J. Mol. Spectrosc.*, 1985, **112**, 211.
30 J. H. Van Vleck, *Phys. Rev.*, 1929, **33**, 467.
31 H. Lefevre-Brion, R. W. Field, *Perturbations in the Spectra of Diatomic Molecules*, Academic, London, 1986, p. 139–145.
32 J. S. Baskin and A. H. Zewail, *J. Phys. Chem.*, 1989, **93**, 5701.
33 A. J. Gotch and T. S. Zwier, *J. Chem. Phys.*, 1990, **93**, 6977.
34 Th. Weber, A. M. Smith, E. Riedle, H. J. Neusser and E. W. Schlag, *Chem. Phys. Lett.*, 1990, **175**, 79.
35 M. Schäfer and D. W. Pratt, *J. Chem. Phys.*, 2001, **115**, 11 147.
36 E. Cané, A. Miani, P. Palmieri, R. Tarroni and A. Trombetti, *J. Chem. Phys.*, 1997, **106**, 9004.
37 J. D. Augspurger, C. E. Dykstra and T. S. Zwier, *J. Phys. Chem.*, 1992, **96**, 7252.
38 J. K. Gregory and D. C. Clary, *Mol. Phys.*, 1996, **88**, 33.